Particle Accelerators, 1988, Vol. 23, pp. 167–185
Reprints available directly from the publisher
Photocopying permitted by license only

Printed in the United States of America

BEAM STABILITY IN A SOLENOID-FOCUSED BETATRON†

THOMAS P. HUGHES
Mission Research Corporation, 1720 Randolph Road, S.E. Albuquerque, New Mexico 87106

(Received June 16, 1987; in final form December 11, 1987)

The solenoid-lens betatron uses periodic solenoid focusing to increase the current that can be injected into a betatron. A dispersion relation for the negative-mass instability in this device is derived using a multiple-length-scale method to average over the nonuniform toroidal field. The result qualitatively resembles the dispersion relation for the conventional betatron but has a finite transition energy and suppressed growth rates. Both effects are due to the solenoid focusing. It is shown that for a space-charge-dominated equilibrium, finite beam radius has a strong stabilizing influence even in the absence of an energy spread. Results of 3-D numerical simulations confirm the predicted stability at low toroidal-mode numbers. High toroidal-mode numbers show anomalously large growth rates but saturate nonlinearly in a relatively benign manner.

1. INTRODUCTION

Several types of betatronlike accelerators for high-current charged particle beams are being studied at present.[1–6] In order to overcome the space-charge limit on the current at low energies, these devices apply external magnetic fields in addition to those of the conventional betatron.[7] At the Institute for Accelerator and Plasma Beam Technology (IAPBT) of the University of New Mexico (UNM), a device is under construction in which the additional fields take the form of solenoid lenses,[5,6] as shown in Fig. 1. Forty solenoids of alternating polarity are arranged around a racetrack-shaped drift tube. Thus, in contrast to the "modified" betatron,[1] which has a uniform toroidal magnetic field, the toroidal field in the IAPBT betatron alternates in direction from one solenoid to the next, with a magnetic cusp between each pair of solenoids. The advantages of this configuration have been discussed by Humphries *et al.*[5,6]

In this paper, we consider the negative-mass instability[8] in the presence of solenoid lenses. This instability has been shown to be important for high-current electron beams in the modified betatron,[9,10] and stellatron,[11] potentially causing serious disruption during the time it takes to accelerate the beam. Derivation of a negative-mass instability dispersion relation for the solenoid-lens betatron is complicated due to the lack of toroidal symmetry. To deal with this problem, we use a multiple-length-scale method to average over the varying solenoid fields.

† This work was supported by the Office of Naval Research.

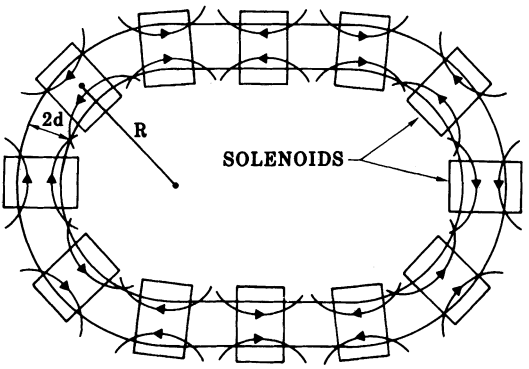

FIGURE 1 Conceptual picture of the solenoid-lens betatron. In the actual device, 40 solenoids are placed around the racetrack.

This leads to a dispersion relation like that for the conventional betatron,[8] with a modified transverse focusing term. The nature of the beam equilibrium in the solenoid-lens betatron results in a considerable spread in particle circulation frequencies at low beam energies. We evaluate the stabilizing effect of this spread on the negative-mass instability. The analytic results are compared to three-dimensional particle-in-cell code simulations. These simulations do not make use of the multiple-length-scale approximation and so can be run at short wavelengths, where this approximation breaks down.

This paper is organized as follows. In Section 2, we obtain the equations for the equilibrium and small-amplitude motion of the beam. In Section 3, we derive a dispersion relation for the negative-mass instability including the effect of the solenoid lenses. In Section 4, we calculate the effect of circulation frequency spread. In Section 5, we present some results of particle simulations of the negative-mass instability in a solenoid-lens betatron. Our conclusions are given in Section 6.

We shall use a system of normalized units that are convenient for electron beam physics problems. A plasma frequency ω_{p0} is defined such that $c/\omega_{p0} =$ 1 cm, where c is the velocity of light. Then length is normalized to c/ω_{p0}, time to $1/\omega_{p0}$, velocities to c, densities to $\omega_{p0}^2 m/4\pi e^2$, and electric and magnetic fields to $mc\omega_{p0}/e$, where e and m are the electronic charge and mass, respectively.

2. BEAM EQUILIBRIUM

For the purposes of this paper, we will assume that the accelerator drift tube is a torus rather than a racetrack. (The IAPBT device has a modular design, and can be configured either as a racetrack or as a torus.[5,6]) The coordinates we use are shown in Fig. 2. The reference orbit is that of a particle at $r = R$, $z = 0$. For this particle,

$$R = \gamma_0 V / B_{z0}, \tag{1}$$

where B_{z0} is the value of the vertical field at $r = R$, γ_0 is the matched particle energy, and $V = (1 - 1/\gamma_0^2)^{1/2}$. If we displace the particle from this orbit, then its

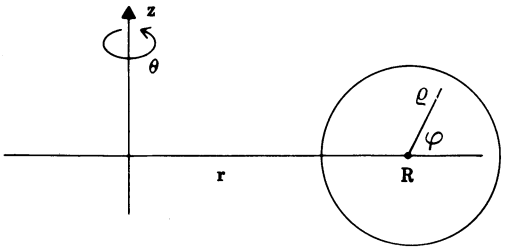

FIGURE 2 The coordinates used in the analytic derivation are cylindrical (r, θ, z) and toroidal $(\varrho, \varphi, \theta)$.

equations of motion are

$$
\begin{aligned}
-\frac{\gamma V_\theta^2}{r}+\frac{dp_r}{dt} &= E_r + V_\theta B_z - V_z B_\theta, \\
\gamma\frac{V_\theta V_r}{r}+\frac{dp_\theta}{dt} &= E_\theta + V_z B_r - V_r B_z, \\
\frac{dp_z}{dt} &= E_z + V_r B_\theta - V_\theta B_r,
\end{aligned}
\tag{2}
$$

where the components of the vectors **V**, **p**, **E**, **B**, represent velocity, momentum, and electric and magnetic fields, respectively. We now proceed to linearize these equations about the reference orbit in the paraxial approximation.[12] For a particle at position $r = R + \delta r$, $z = \delta z$, the applied fields are

$$
\begin{aligned}
B_z &= B_{z0}(1 - n\delta r/R) + B_{zs}, \\
B_r &= -B_{z0} n\delta z/R + B_{rs}, \\
B_\theta &= B_{\theta s},
\end{aligned}
\tag{3}
$$

where n is the external field index, $n = -(R/B_{z0})\, dB_z/dr$, and subscript s denotes terms due to the solenoid magnets. The fields B_{zs}, B_{rs}, $B_{\theta s}$ are periodic in θ and can all be obtained from a single component of a vector potential [see Eq. (7)]. For the moment, we assume the beam is in a region of uniform toroidal field, where B_{rs}, B_{zs} can be neglected. If we assume a Kapchinsky–Vladimirsky (KV)[12] beam equilibrium that has an elliptical cross section (we will show that this is consistent later) then the self fields at the particle can be calculated from the static Maxwell's equations:

$$
\begin{aligned}
E_r &= \frac{n_0 b}{a+b}\,\delta r, \\
E_z &= \frac{n_0 a}{a+b}\,\delta z, \\
B_z^s &= -\frac{n_0 V b \delta r}{a+b}, \\
B_r^s &= \frac{n_0 V a \delta z}{a+b},
\end{aligned}
\tag{4}
$$

where a and b are the radii in the r and z directions, respectively, n_0 is the beam density, and superscript s denotes "self field." Combining these equations with the linearizations of Eqs. (2), we obtain

$$\begin{aligned} \delta\ddot{r} + \left(1 - n - \frac{2n_s b}{a+b}\right)\omega_0^2 \delta r + \delta\dot{z}\frac{B_{\theta s}}{\gamma_0} = 0, \\ \delta\ddot{z} + \left(n - \frac{2n_s a}{a+b}\right)\omega_0^2 \delta z - \delta\dot{r}\frac{B_{\theta s}}{\gamma_0} = 0, \end{aligned} \tag{5}$$

where $\omega_0 = V/R$, and the quantity $n_s \equiv 2\nu R^2/\gamma_0^3 V^2 ab$ is referred to as the self-field index (ν is Budker's parameter, $I_b = 17\nu VkA$). For a self-consistent cold KV equilibrium, the radii a and b are chosen such that

$$1 - n - \frac{2n_s b}{a+b} = n - \frac{2n_s a}{a+b}. \tag{6}$$

To treat the effect of the magnetic cusps, it is convenient to change the coordinate system to the toroidal coordinates shown in Fig. 2 and introduce a vector potential $A_{\varphi s}(\theta)$ that describes the solenoid field. Equations (5) are replaced by

$$\ddot{\varrho} - \varrho\dot{\varphi}^2 + \omega_\varrho^2 \varrho + \varrho\dot{\varphi}\frac{B_{\theta s}}{\gamma_0} = 0, \tag{7a}$$

$$\frac{1}{\varrho}\frac{d}{dt}[\varrho(\varrho\dot{\varphi} + A_{\varphi s})] = 0, \tag{7b}$$

where

$$\omega_\varrho^2 = \left(1 - n - \frac{2n_s b}{a+b}\right)\omega_0^2.$$

Equation (7b) can be integrated to obtain

$$L = \varrho^2\dot{\varphi} + \frac{\varrho A_{\varphi s}}{\gamma_0} = \varrho^2\left(\dot{\varphi} - \frac{1}{2}\frac{B_{\theta s}}{\gamma_0}\right) = \text{const.} \tag{8}$$

Since L is a constant, its value is determined by the initial conditions. Experimentally, the beam will be generated using a cathode shielded from magnetic fields,[5,6] so that $L = 0$. Substituting this into Eq. (7a), we obtain

$$\ddot{\varrho}\left(\frac{1}{4}\frac{B_{\theta s}^2}{\gamma_0^2} + \omega_\varrho^2\right)\varrho = 0. \tag{9}$$

In the limit that the cusps become infinitely sharp, $B_{\theta s}^2$ is a constant over the particle orbit, and Eq. (9) has a stationary solution for

$$\omega_\varrho^2 + \frac{1}{4}\frac{B_{\theta s}^2}{\gamma_0^2} = 0. \tag{10}$$

This is the condition for a space-charge dominated equilibrium, i.e., one where the emittance is negligible. To be consistent with the assumption of a fixed

equilibrium profile, we require that the "phase advance per solenoid," i.e., the poloidal angle through which the particles rotate on going through one solenoid, be small:

$$\mu_0 = \frac{1}{2}\frac{B_{\theta s}}{\gamma_0}\frac{S}{V} \ll 1, \tag{11}$$

where S is the length of a solenoid. The case $n = 1/2$ is a special one, since $a = b$, and poloidal rotation does not affect the beam profile. In this case, Eq. (11) can be relaxed. Struckmeier and Reiser[13] have shown that $\mu_0 < \pi/2$ is required for envelope stability.

Physically, the equilibrium we have just constructed behaves as follows. In a given solenoid, the beam particles rotate poloidally at the Larmor frequency, $B_{\theta s}/2\gamma_0$. On passing through the magnetic cusp into the next solenoid, the poloidal rotation changes direction. The shape of the beam is elliptical, in general, with radii determined from Eq. (6), and the beam has a uniform density determined from Eq. (10). If the magnetic cusps are not infinitely sharp, then an equilibrium can still be constructed,[13] but the radii a and b vary periodically with toroidal angle.

3. NEGATIVE-MASS INSTABILITY

In order to analyze the negative-mass instability, we adopt a simplified model of the beam dynamics. We assume that the beam acts like a rigid body in the transverse direction, so that only the transverse motion of the beam centroid has to be calculated, rather than the transverse motion of each beam particle. Comparisons between a rigid-beam model and three-dimensional particle simulations for the case of the modified betatron[9] have produced good agreement. The physical basis for the model rests on the fact that when the beam minor radius is much smaller than the drift-tube minor radius, then the perturbed toroidal forces are the same for all particles in a given transverse slice of the beam, and the perturbed transverse forces are linearly proportional to the transverse displacement of each particle in the slice. In the toroidal direction, the model places no restriction on the beam motion. The transverse motion of the beam generates perturbed dipole fields, whereas toroidal bunching generates perturbed monopole fields.

To obtain the equations for the perturbed beam centroid motion, we linearize Eqs. (2). The perturbed position of a transverse slice of the beam is given by

$$\mathbf{r} = [R + \Delta r(\theta_0, t)]\hat{r} + \Delta z(\theta_0, t)\hat{z} + \Delta\theta(\theta_0, t)\hat{\theta}$$

where $\theta_0(t)$ is the unperturbed θ-position, Δr, Δz, and $\Delta\theta$ are the so-called polarization variables,[11,14] and $\hat{r}$, $\hat{z}$, and $\hat{\theta}$ are unit vectors located at the unperturbed position. The field quantities that we insert into these equations are evaluated at the center of the beam. It has been shown[9] that toroidal corrections to the continuity equation and the field equations (i.e., terms of order d/R and

higher where d is the wall radius) must be retained in the calculation, particularly for high toroidal-mode numbers. A model that uses an exact, though cumbersome, solution to these equations has been derived.[15] The exact model shows that the cylindrical approximation for the field equations gives reasonably good results for low toroidal-mode numbers if a certain replacement is made [Eq. (30)]. Here, we will make use of this simplification in order to avoid the complexities of toroidal corrections.

For low toroidal-mode numbers, the long-wavelength, low-frequency approximation $\omega^2,\ l^2/R^2 \ll \nabla_\perp^2$ (ω and l denote the mode frequency and wave number, respectively, and $\nabla_\perp^2$ denotes the transverse Laplacian) can be used in solving the field equations. Neglecting toroidal corrections and assuming a circular beam cross section, the solutions for the perturbed transverse self fields at the perturbed beam centroid position are

$$\begin{aligned}
\Delta E_r &= \frac{n_0}{2}\frac{a^2}{d^2}\Delta r, \\
\Delta E_z &= \frac{n_0}{2}\frac{a^2}{d^2}\Delta z, \\
\Delta B_r^s &= \frac{n_0 V}{2}\frac{a^2}{d^2}\Delta z, \\
\Delta B_z^s &= -\frac{n_0 V}{2}\frac{a^2}{d^2}\Delta r,
\end{aligned} \tag{12}$$

where Δ denotes perturbed quantities. These fields come from the dipole components of $\Delta\mathbf{E}_\perp$ and $\Delta\mathbf{B}_\perp^s$. The monopole components of the transverse fields do not couple to the centroid motion. The monopole component of ΔE_θ does enter, however, and can be obtained using the integral form of Faraday's Law,

$$\begin{aligned}
&\oint \mathbf{E}\cdot\mathbf{dl} = -\frac{\partial}{\partial t}\int \mathbf{B}\cdot\mathbf{dS}, \\
&\Rightarrow \Delta E_\theta^0 = -\frac{1}{R}\frac{\partial}{\partial\theta}\int_0^d \Delta E_\rho^0\,\mathrm{d}\varrho - \frac{\partial}{\partial t}\int_0^d \Delta B_\varphi^0\,\mathrm{d}\varrho,
\end{aligned} \tag{13}$$

where the superscript zero denotes the monopole component. The sources for ΔE_ρ^0, ΔB_φ^0 are the monopole components of Δn and ΔJ_θ, respectively. The latter are related to the perturbed beam displacement through the continuity equation[9]:

$$\Delta n = -\frac{\partial}{\partial z}n_0\Delta z - \frac{1}{r}\frac{\partial}{\partial r}rn_0\Delta r - \frac{\partial}{\partial\theta}n_0\Delta\theta. \tag{14}$$

From this and $\Delta J_\theta = n_0 R\dot{\Delta}\theta + \Delta n V$, where the dot denotes the total time derivative, we obtain the expressions

$$\begin{aligned}
\Delta n^0 &= -\frac{\partial}{\partial\theta}n_0\Delta\theta, \\
\Delta J_\theta^0 &= \frac{\partial}{\partial t}n_0\Delta\theta.
\end{aligned} \tag{15}$$

Consistent with our use of the cylindrical approximation, we have neglected toroidal terms in Eq. (15). Substitution into Eq. (13) yields

$$\Delta E_\theta^0 = \frac{1}{4} n_0 a^2 \left(1 + 2 \ln \frac{d}{a}\right)\left(\frac{1}{R^2}\frac{\partial^2}{\partial \theta^2} - \frac{\partial^2}{\partial t^2}\right)\Delta\theta . \tag{16}$$

The applied fields are given by Eq. (3), with δr and δz replaced by Δr and Δz. We can now write down the linearized equations of motion for the beam centroid:

$$\begin{aligned} &\Delta\ddot{r} + \omega_\perp^2 \Delta r + \Delta\dot{z}\frac{B_{\theta s}}{\gamma_0} - \frac{\Delta V_\theta B_{zs}}{\gamma_0} = \gamma_0^2 \omega_0 \Delta V_\theta , \\ &\Delta\ddot{z} + \omega_\perp^2 \Delta z - \Delta\dot{r}\frac{B_{\theta s}}{\gamma_0} + \frac{\Delta V_\theta B_{rs}}{\gamma_0} = 0 , \\ &\Delta\dot{V}_\theta = \frac{\Delta E_\theta}{\gamma_0^3} , \end{aligned} \tag{17}$$

where

$$\omega_\perp^2 = \left(\frac{1}{2} - n_s \frac{a^2}{d^2}\right)\omega_0^2 ,$$

and we have taken $n = 1/2$ to be consistent with $a = b$ [Eq. (6)]. To solve Eqs. (17), we perform a multiple-length-scale analysis to average over the solenoid lenses. This involves an ordering scheme where the wavelength of the beam mode λ is assumed to be much longer than the period of the alternating solenoid fields, i.e., $S/\lambda = 0(\varepsilon)$, where ε is a smallness parameter. Consistent with this, we assume $\partial/\partial t$, ω_0, and $\omega_\perp$ are of order ε. In addition, we assume that $\mu_0 \ll 1$ [Eq. (11)]. It is convenient to perform the averaging in toroidal variables ρ, $\phi(\Delta r = \rho\cos\phi,\ \Delta z = \rho\sin\phi)$ in which Eqs. (17) have the form

$$\ddot{\rho} - \rho\dot{\phi}^2 + \omega_\perp^2 \rho + \rho\dot{\phi}\frac{B_{\theta s}}{\gamma_0} = \gamma_0^2 \omega_0 \Delta V_\theta \cos\phi , \tag{18a}$$

$$\frac{1}{\rho}\frac{d}{dt}\left[\rho^2\left(\dot{\phi} - \frac{1}{2}\frac{B_{\theta s}}{\gamma_0}\right)\right] = -\gamma_0^2 \omega_0 \Delta V_\theta \sin\phi , \tag{18b}$$

$$\ddot{\xi} + \omega_0 \Delta\dot{r} - C\left(\frac{\partial^2}{\partial s^2} - \frac{\partial^2}{\partial t^2}\right)\zeta = 0 , \tag{18c}$$

where $\zeta = R\Delta\theta$, $s = R\theta$, and $C = 1/4(n_0 a^2)(1 + 2\ln d/a)/\gamma_0^3$. All quantities are expanded in powers of ε in the following manner,

$$\rho(s, t) = \rho_0(s_0, s_1, t) + \varepsilon\rho_1(s_0, s_1, t) + \ldots , \tag{19a}$$

$$\phi(s, t) = \phi_0(s_0, s_1, t) + \varepsilon\phi_1(s_0, s_1, t) + \ldots , \tag{19b}$$

$$\zeta(s, t) = \zeta_0(s_0, s_1, t) + \varepsilon\zeta_1(s_0, s_1, t) + \ldots , \tag{19c}$$

where s_0, s_1 denote the short and long length scales, respectively. The essence of the multiple-scale method is that s_0 and s_1 are treated as independent variables.

The total time derivative d/dt is expanded as $V(\partial/\partial s_0) + \varepsilon(d/dt_1)$, where $d/dt_1 = \partial/\partial t + V\,\partial/\partial s_1$. To zero order in ε, Eqs. (18) become

$$V^2 \frac{\partial^2}{\partial s_0^2}\rho_0 - \rho_0\left(V\frac{\partial \phi_0}{\partial s_0}\right)^2 = 0,$$

$$V\frac{\partial}{\partial s_0}\left(\rho_0^2 V \frac{\partial \phi_0}{\partial s_0}\right) = 0, \tag{20}$$

$$V^2 \frac{\partial^2}{\partial s_0^2}\zeta_0 - C\frac{\partial^2}{\partial s_0^2}\zeta_0 = 0.$$

From these, we conclude that ρ_0, ϕ_0, and ζ_0 do not depend on s_0. Using this information, we obtain to order ε,

$$V^2 \frac{\partial^2 \rho_1}{\partial s_0^2} = 0,$$

$$\frac{\partial}{\partial s_0}\left[\rho_0^2\left(V\frac{\partial \phi_1}{\partial s_0} + \frac{\partial \phi_0}{\partial t}\right) - \frac{1}{2}\frac{B_{\theta s}}{\gamma_0}\right] = 0, \tag{21}$$

$$(V^2 - C)\frac{\partial^2}{\partial s_0^2}\zeta_1 = 0,$$

These equations imply that ρ_1 and ζ_1 also do not depend on s_0. For ϕ_1, we obtain

$$\phi_1 = \left[\frac{F(t, s_1)}{\rho_0^2} - \frac{\partial \phi_0}{\partial t}\right]s_0 + \frac{1}{2}\int \frac{B_{\theta s}}{\gamma_0}\,ds_0 + G(t, s_1), \tag{22}$$

where $F(t, s_1)$, $G(t, s_1)$ are arbitrary constants. The secular dependence on s_0 can be removed by choosing

$$F = \rho_0^2 \frac{\partial \phi_0}{\partial t}. \tag{23}$$

This choice implies that $\partial \phi_1/\partial s_0 = B_{\theta s}/\gamma_0$ depends *only* on s_0. Here we are making use of the fact that the toroidal field reverses from one solenoid to the next, so that, unlike the modified betatron, the toroidal field has no long-wavelength component. We shall see that this difference results in a dispersion relation that is qualitatively different from that of the modified betatron.[9,10] Proceeding to order ε^2, we obtain

$$V^2\frac{\partial^2 \rho_2}{\partial s_0^2} + \frac{\partial^2 \rho_0}{\partial t^2} - \rho_0\left(\frac{\partial \phi_0}{\partial t} + V\frac{\partial \phi_1}{\partial s_0}\right)^2$$
$$+ \omega_\perp^2 \rho_0 + \rho_0\left(\frac{\partial \phi_0}{\partial t} + V\frac{\partial \phi_1}{\partial s_0}\right)\frac{B_{\theta s}}{\gamma_0} = \gamma_0^2 \omega_0\left(\omega_0 \rho_0 \cos\phi_0 + \frac{\partial \zeta_0}{\partial t}\right)\cos\phi_0, \tag{24a}$$

$$V^2\frac{\partial^2 \phi_2}{\partial s_0^2} + \frac{\partial}{\partial t}\left(\rho_0^2 \frac{\partial \phi_0}{\partial t}\right) = -\gamma_0^2 \omega_0\left(\frac{\partial \zeta_0}{\partial t} + \omega_0 \rho_0 \cos\phi_0\right)\sin\phi_0, \tag{24b}$$

$$V^2\frac{\partial^2}{\partial s_0^2}\zeta_2+\frac{\partial^2\zeta_0}{\partial t^2}+\omega_0\left(\frac{\partial}{\partial t}\rho_0\cos\phi_0-V\rho_0\sin\phi_0\frac{\partial\phi_1}{\partial s_0}\right)$$
$$-C\left[\frac{\partial^2\zeta_2}{\partial s_0^2}+\left(\frac{\partial^2}{\partial s_1^2}-\frac{\partial^2}{\partial t^2}\right)\zeta_0\right]=0. \quad (24c)$$

We now average these equations over one period of the magnetic lenses. Subtracting the averaged equations for Eqs. (24b) and (24c) from the unaveraged ones, we obtain,

$$\frac{\partial^2\phi_2}{\partial s_0^2}=\left\langle\frac{\partial^2\phi_2}{\partial s_0^2}\right\rangle, \quad (25a)$$

$$(V^2-C)\frac{\partial^2\zeta_2}{\partial s_0^2}=(V^2-C)\left\langle\frac{\partial^2\zeta_2}{\partial s_0^2}\right\rangle+V\omega_0\rho_0\sin\phi_0\frac{\partial\phi_1}{\partial s_0}, \quad (25b)$$

where the brackets $\langle\ \rangle$ denote the average. Solving these equations, and removing secularities in the usual way, we find $\partial^2\phi_2/\partial s_0^2=\langle\partial^2\zeta_2/\partial s_0^2\rangle=0$. From Eq. (24b), we note that if we impose the initial conditions $\phi_0=0$, $\partial\phi_0/\partial t=0$ at $t=0$, then this equation has the unique solution $\phi_0(t)=0$. By imposing these initial conditions, and thereby restricting the class of initial conditions for which the analysis is valid, we can set $\phi_0=0$ in Eqs. (24). From Eqs. (22) and (24a), we then obtain

$$V^2\frac{\partial^2\rho_2}{\partial s_0^2}+\frac{\partial^2\rho_0}{\partial t^2}+\frac{1}{4}\left\langle\frac{B_{\theta s}}{\gamma_0}\right\rangle^2\rho_0+\omega_\perp^2\rho_0=\gamma_0^2\omega_0\left(\omega_0\rho_0+\frac{\partial\zeta_0}{\partial t_1}\right). \quad (26)$$

By subtracting this equation from its average, it is again straightforward to show that $\langle\partial^2\rho_2/\partial s_0^2\rangle=0$ (but $\partial^2\rho_2/\partial s_0^2\neq 0$). We thereby obtain the equations for the averaged beam centroid motion:

$$\frac{\partial^2\rho_0}{\partial t^2}+\left(\omega_\perp^2+\frac{1}{4}\left\langle\frac{B_{\theta s}^2}{\gamma_0^2}\right\rangle\right)\rho_0=\gamma_0^2\omega_0\left(\omega_0\rho_0+\frac{\partial\zeta_0}{\partial t}\right), \quad (27a)$$

$$\frac{\partial^2\zeta_0}{\partial t^2}+\omega_0\frac{\partial\rho_0}{\partial t}-C\left(\frac{\partial^2}{\partial s_1^2}-\frac{\partial^2}{\partial t^2}\right)\zeta_0=0, \quad (27b)$$

$$\phi_0=0. \quad (27c)$$

Note that Eqs. (27a) and (27b) have the form of the equations one would obtain if no solenoid magnetic lenses were present. Thus, to the order we have solved the original equations, the net effect of the solenoid lenses is to increase the transverse focusing on the beam by an amount proportional to $\langle B_{\theta s}^2/\gamma_0^2\rangle$, i.e.,

$$\omega_\perp^2\rightarrow\omega_\perp^2+\frac{1}{4}\left\langle\frac{B_{\theta s}^2}{\gamma_0^2}\right\rangle\equiv\Omega_\perp^2. \quad (28)$$

To obtain a dispersion relation from Eqs. (27), we assume that the perturbed quantities vary as $\exp(il\theta-i\omega t)$. In Eq. (27b), we obtain the factor $l^2/R^2-\omega^2$. However, as shown in Ref. 15, when toroidal corrections to the field equations and the continuity equation are kept, we instead obtain the factor $\alpha_1 l^2/R^2-$

$\alpha_2\omega^2$, where α_1 and α_2 are frequency- and mode-number-dependent expressions approximately equal to unity. In general, we can approximate $\omega = l\omega_0$ in evaluating this factor,

$$\alpha_1 \frac{l^2}{R^2} - \alpha_2\omega^2 \approx \frac{l^2}{R^2}(\alpha_1 - \alpha_2 V^2). \tag{29}$$

Small differences between α_1 and α_2 can strongly affect the magnitude and even the sign of $\alpha_1 - \alpha_2 V^2$. These effects become increasingly evident as the mode number l increases. However, the averaging procedure we have used is only valid for low mode numbers, and for our purposes it will be sufficient to set $\alpha_1 = \alpha_2 = 1$ in Eq. (29):

$$\alpha_1 \frac{l^2}{R^2} - \alpha_2\omega^2 \approx \frac{1}{\gamma_0^2}\frac{l^2}{R^2}. \tag{30}$$

This approximation was made on heuristic grounds by Landau and Neil.[8] The main error introduced is in the asymptotic falloff of growth rate with γ_0.[15] The important point here is that much larger errors are introduced by keeping the unmodified factor $l^2/R^2 - \omega^2$ in the dispersion relation. Fictitious cutoffs in the growth rate as a function of energy and current are predicted.[16]

Using Eq. (30), the dispersion relation obtained is

$$1 = \frac{l^2 C}{R^2\Omega^2}\left(\frac{1}{\gamma_0^2} + \frac{\omega_0^2}{\Omega^2 - \Omega_\perp^2}\right), \tag{31}$$

where $\Omega = \omega - l\omega_0$.

4. SOLUTIONS TO THE DISPERSION RELATION

By inspection of Eq. (31), we see that there are resonances at $\Omega^2 = 0$ and $\Omega^2 = \Omega_\perp^2$, corresponding to the longitudinal and transverse modes of oscillation of the beam. These modes are coupled through the negative-mass effect. For the low l-numbers we are considering, the coupling is non-resonant, i.e., the resonances do not overlap. Thus, for the mode near $\Omega = 0$, we can set $\Omega^2 \ll \Omega_\perp^2$, to get

$$\Omega^2 = \frac{l^2 C}{R^2}\left(\frac{1}{\gamma_0^2} - \frac{\omega_0^2}{\Omega_\perp^2}\right) \equiv -\Gamma_0^2. \tag{32}$$

When the right-hand side is negative, we obtain the negative-mass instability. For $B_{\theta s} = 0$, Eq. (32) becomes the expression of Landau and Neil[8] for a monoenergetic beam in a conventional betatron. Equation (32) together with Eqs. (10), (17), and (28) give the condition for instability as

$$\gamma_0 > \left(\frac{1}{2} + \frac{1}{4}\frac{\langle B_{\theta s}^2/\gamma_0^2\rangle}{\omega_0^2}\right)^{1/2}\left(1 - \frac{a^2}{d^2}\right)^{1/2} \equiv \gamma_t. \tag{33}$$

Thus, the strong-focusing effect of the solenoids introduces a finite negative-mass transition energy γ_t below which the beam is stable. This contrasts with the

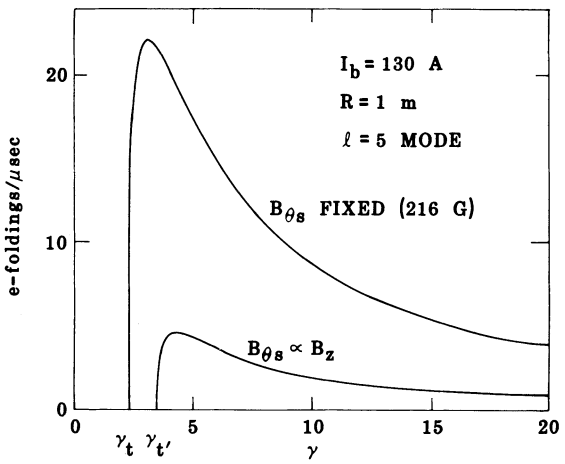

FIGURE 3 Growth rates of the $l = 5$ negative-mass instability obtained from Eq. (31) for the parameters in Table I.

conventional betatron, which is unstable at all energies. Further, we note from Eq. (32) that when $\langle B_{\theta s}^2/\gamma_0^2 \rangle \gg 1/2$, the growth rate scales as $1/|B_{\theta s}|$, so that the solenoid focusing strongly suppresses growth of the instability.

As the beam is accelerated, γ_0 increases. We see from Eq. (28) that the effect of the solenoid focusing rapidly decreases unless $B_{\theta s}$ is increased also. By ramping $B_{\theta s}$ in synchronism with γ_0, the suppression of growth rates relative to the conventional betatron is maintained. An additional benefit is that the crossing of single-particle resonances is avoided. The obvious drawback is that additional energy is required to drive the solenoids.

In Fig. 3 we show growth rates obtained from Eq. (31) for parameters typical of the IAPBT betatron (Table I). The curves show the contrast between a case where the solenoid field is kept fixed at its injection value, and one where it is ramped linearly with γ_0. Note that the growth rates in both cases are substantial for a device with an acceleration time of several tens of microseconds.

There is a qualitative difference between Eq. (31) and the corresponding

TABLE I

Solenoid Lens Betatron Parameters

Torus major radius	1 m
Torus minor radius	4.5 cm
Beam major radius	1 m
Beam minor radius (at injection)	~2 cm
Injected beam energy	300 kV
Injected beam current	~100 A
Solenoid field amplitude (at injection)	~220 gauss
Number of solenoids	30

dispersion relation for the modified betatron,[1,10] which has a uniform toroidal field. In Eq. (31) only the radial and toroidal modes of the beam are coupled (see Fig. 7). In the modified betatron, the radial beam motion is coupled to the vertical motion (z-direction in Fig. 2) as well as to the toroidal motion.

5. STABILIZATION DUE TO FINITE BEAM RADIUS

In the derivation of Eq. (31), we assumed that all particles rotate about the major axis of the torus at the same frequency, namely, $\omega_0 = V/R$. For a finite-radius beam, however, there is a spread in path lengths around the torus. thus, even if $V = c$ for all particles, there is a spread in rotation frequencies. Taking a uniform density equilibrium of the type discussed in Section 2, with circular cross section and small phase advance per solenoid (Eq. 11), it is straightforward to show that the distribution function for the particle rotation frequencies is

$$F(\dot{\theta}) = A[a^2\omega_0^2/R^2 - (\dot{\theta} - \omega_0)^2]^{1/2}, \tag{34}$$

where A is a normalization constant and $\dot{\theta}$ is the particle rotation frequency. The width of the distribution function is $a\omega_0/R$. This contrasts with the conventional and modified betatrons, where the betatron oscillations of the particles result in a width that is only of order $(a/R)^2$ for a monoenergetic beam (see Fig. 4). For these devices, it is generally necessary to have an energy spread on the beam to obtain a significant frequency spread.[8,10]

In order to derive a dispersion relation taking frequency spread into account, a kinetic treatment is necessary. Rather than redoing the analysis of Section 3 in the framework of the Vlasov equation, we will make a plausibility argument for adapting the kinetic dispersion relation for the conventional betatron derived by Landau and Neil.[8] As observed in Section 4, Eq. (31) can be obtained from the cold-beam result of Ref. 8 when the replacement in Eq. (28) is made. The longitudinal motion of the particles is affected by the solenoid only to order $(\mu_0 a/S)^2 \ll 1$. Therefore, we expect the influence of the solenoids on the resonance at $\Omega^2 = 0$, which is associated with the instability, to be minimal. In

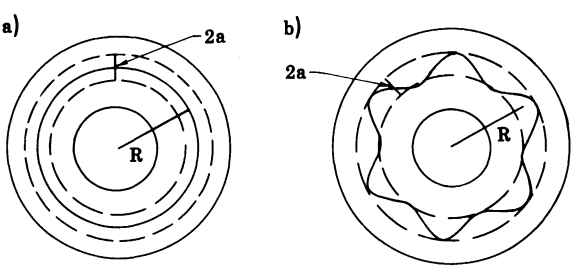

FIGURE 4 An equilibrium in which there is little transverse oscillation of the particles (as in a) has a much greater frequency spread than an equilibrium in which the radius is determined by the amplitude of betatron oscillations (as in b).

addition, as noted at the beginning of Section 4, there is no resonant coupling to the transverse beam modes for low l-numbers. On this basis, we modify the kinetic equation of Ref. 8 according to Eq. (28), and obtain the dispersion relation:

$$1 = -\left[\frac{1}{4}\frac{a^2}{\gamma_0^2}\left(1 + 2\ln\frac{d}{a}\right)\right]\int \frac{\partial f}{\partial p}\frac{l\,dp}{\Omega + lk\tilde{p}}, \tag{35}$$

where

$$k = \frac{1}{\gamma_0 R^2}\left(\frac{\omega_0^2}{\Omega_\perp^2} - \frac{1}{\gamma_0^2}\right);$$

$p = \gamma\omega_0 R^2 + \tilde{p}$ is the canonical angular momentum, and f is normalized such that $\int f dp = n_0$. The relation between $\tilde{p}$ and $\dot{\theta}$ is $\dot{\theta} = \omega_0 - k\tilde{p}$. Converting Eq. (35) into an integral over $\dot{\theta}$, and inserting the distribution function in Eq. (34), we obtain the dispersion relation

$$1 = G\left\{1 + \frac{\Omega}{[\Omega^2 - (la\omega_0/R)^2]^{1/2}}\right\}, \tag{36}$$

where

$$G = \frac{2C}{R^2}\left(\frac{\omega_0^2}{\Omega_\perp^2} - \frac{1}{\gamma_0^2}\right)\left(\frac{R^2}{a^2\omega_0^2}\right).$$

Equation (36) can be made analytic in the complex ω plane by introducing the branch cut shown in Fig. 5. We find that for $1 < G < \infty$, the beam is unstable with growth rate

$$\Gamma = \frac{l\omega_0 a}{R}\frac{G-1}{\sqrt{2G-1}}. \tag{37}$$

The zero-frequency-spread growth rate Γ_0 in Eq. (32) can be recovered by letting $a \to 0$. As G approaches 1 from above, the roots approach the branch cut, as

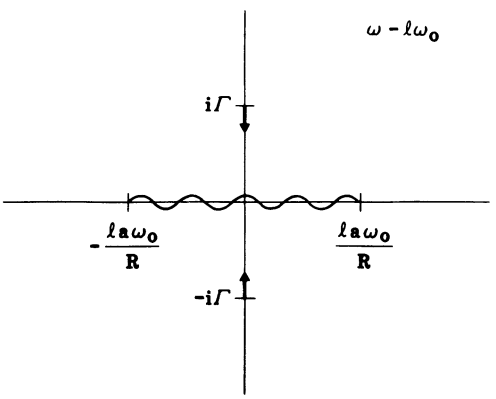

FIGURE 5 Branch cut in the complex $\omega - l\omega_0$ plane to make the dispersion relation, Eq. (36), analytic. The arrows show the movement of the roots as $G \to 1$ from above.

shown in Fig. 5. For $G < 1$, the negative-mass mode disappears, and the beam is stable. The stability criterion can be rewritten

$$\Gamma_0 \leqslant \frac{l\omega_0 a}{R}. \tag{38}$$

This criterion has a physical interpretation in terms of the rotation frequency spread of the particles. Consider two particles, one at $r = R$, and one at $r = R \pm a$, which are initially at the same toroidal angle. Then at marginal stability, these particles will become separated by $1/l$ radians in a time $1/\Gamma_0$. This smearing effect prevents clumping of the beam.

We emphasize that the stability criterion just derived is only valid for a cold, space-charge-dominated equilibrium of the type described in Section 2. To apply Eq. (38) to a hot beam, one must calculate an effective radius that excludes the contribution of transverse betatron oscillations to the radius. In the extreme case, where the finite beam radius is completely due to betatron oscillations, as in Fig. 4b, the frequency spread is negligible for typical parameters.

Applying Eq. (38) to the cases in Fig. 3, we find that a beam radius of 1.2 cm is sufficient to stabilize the peak growth rate. As the beam is accelerated, its radius shrinks, thereby decreasing the width of the frequency distribution. From Eq. (10) we find

$$a^2 = \frac{8\nu R^2}{\gamma_0^3 V^2}\left(2 + \frac{\langle B_{\theta s}^2/\gamma_0^2\rangle}{\omega_0^2}\right)^{-1}, \tag{39}$$

so that the radius shrinks as $\gamma_0^{-3/2}$ if $\langle B_{\theta s}^2/\gamma_0^2\rangle$ is held fixed. If $B_{\theta s}$ is held fixed, then the scaling is more complicated at low energy but quickly goes over to a $\gamma_0^{-3/2}$ scaling as γ_0 increases. From Eq. (32), we see that the growth rate Γ_0 also shrinks as $\gamma_0^{-3/2}$. Therefore, if the beam is stable just above the transition energy where Γ_0 is a maximum, then it will tend to remain so as the acceleration proceeds. In addition, both sides of Eq. (38) scale linearly with l, so that if one mode is stable then all modes are. As we shall see in Section 6.1, this scaling breaks down for large l-numbers.

6. COMPARISON WITH NUMERICAL SIMULATIONS

In order to check the analytic theory, and to study the nonlinear effects of the instability, we carried out a limited number of simulations using the three-dimensional particle-in-cell (PIC) code IVORY, which has been used successfully to model the negative-mass instability in the modified betatron.[9,15] The code is fully electromagnetic and advances the complete Lorentz force equations for the particles. A two-dimensional grid is used to represent the transverse plane of the beam, whereas fields in the toroidal direction are represented by a Fourier sum. This allows us to compare predictions for individual l-numbers directly with theory. For economy, we generally keep three or fewer toroidal modes in the simulations. To model the solenoid-lens betatron, a sinusoidally varying toroidal

field is used. We use Eq. (10), with $B_{\theta s}^2/\gamma_0^2$ replaced by $\langle B_{\theta s}^2/\gamma_0^2 \rangle$, to obtain suitable equilibria to initialize the simulations. We find that small-amplitude envelope oscillations are excited because the cusps are not infinitely sharp.[17]

6.1. *IAPBT Parameters*

Three simulations were performed for the parameters in Table I. We assumed 30 solenoids around the torus since 10 of the 40 solenoids in the actual device are on straight sections that we do not simulate here. First, we looked at the $l = 5$ mode at $\gamma_0 = 3$. The beam radius was chosen to be 1.75 cm, for which the matched amplitude of the solenoid field is 134 gauss. The simulation was run for 230 ns, during which no measurable growth was observed. The theoretically predicted growth rate is $22.8\,\mu s^{-1}$, which would have produced about 5.3 *e*-foldings in 230 ns. (This growth rate is higher than those shown in Fig. 3 because of the lower solenoid field.) We attribute the beam stability to the spread in circulation frequencies. The right-hand side of Eq. (38) is $26.2\,\mu s^{-1}$, which is marginally sufficient for stability.

The averaging procedure of Section 4 breaks down as the mode number l approaches the mode number l_s associated with the periodic solenoid field. For our case, $l_s = 15$. Since no averaging is used in the simulation code, however, such modes can be looked at numerically. For the same parameters as the $l = 5$ simulation above, we performed a simulation of the $l = l_s = 15$ mode. We observed a strong instability, with a growth rate of $66\,\mu s^{-1}$, as shown in Fig. 6. A particle plot from the nonlinear stage of the instability (Fig. 7) shows typical negative-mass instability behavior, i.e., radial kinking accompanied by toroidal clumping. The instability has almost saturated at the point reached in Fig. 7, but 1/6 of the current has been scraped off onto the wall. If the wall radius had been larger, the instability might have saturated without current loss.

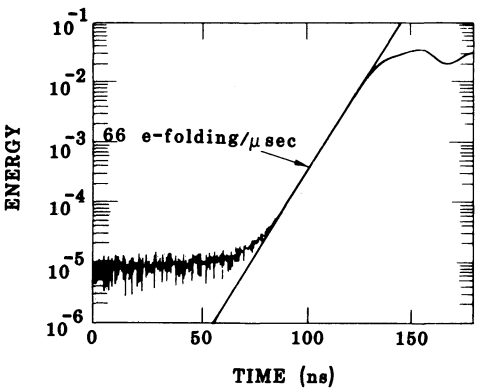

FIGURE 6 Energy history of the $l = 15$ mode in a simulation of a 100-A, $\gamma_0 = 3$ beam, showing the linear growth and nonlinear saturation.

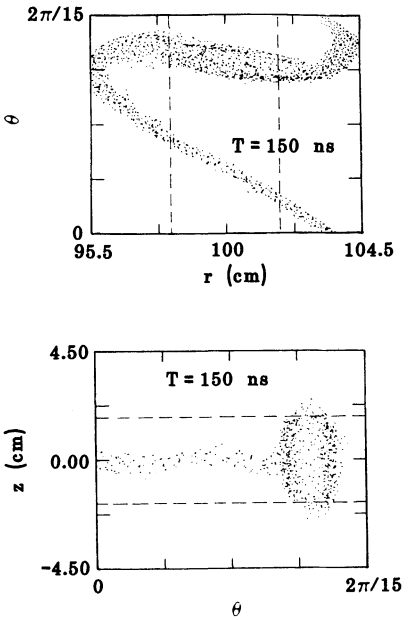

FIGURE 7 Particle plots ($r - \theta$, $z - \theta$) taken during the nonlinear state of the $l = 15$ negative-mass instability on a 100-A, $\gamma_0 = 3$ beam. The dashed lines show the edges of the toroidally uniform beam at the start of the simulation.

If we naively apply the analytic dispersion relation to the $l = 15$ mode, we obtain a growth rate of 66 μs^{-1}, the same as the numerical result. However, Eq. (38) predicts stability due to frequency spread. Thus, it appears that the zero-frequency-spread growth rate for $l = 15$ is significantly larger than that predicted by analytic theory. On the other hand, the analytic prediction of a negative-mass transition energy appears to be valid even for $l = 15$. We simulated this mode for $\gamma_0 = 1.6$, which corresponds to the injection energy of the IAPBT betatron, and observe no instability. Equation (33) predicts stability up to at least $\gamma_0 = 2.2$ (see Fig. 3).

6.2. High-Current Beam Stability

If experiments at 100 A are successful, then higher-current experiments will be undertaken. We have performed three simulations of 10-kA beams to investigate beam stability at high current. We assumed 20 solenoids around a torus with a 1-m major radius and simulated the mode $l = 2 \times l_s = 20$ (this mode was chosen for reasons of computational economy). In Fig. 8, we compare the simulation results with (a) growth rates obtained for a conventional betatron (no toroidal field) and (b) growth rates obtained by using the averaged approximation for the solenoid lenses. Because of the high l-number, the curves in Fig. 8 were obtained by inserting Eq. (28) into the exact analytic dispersion relation for a conventional

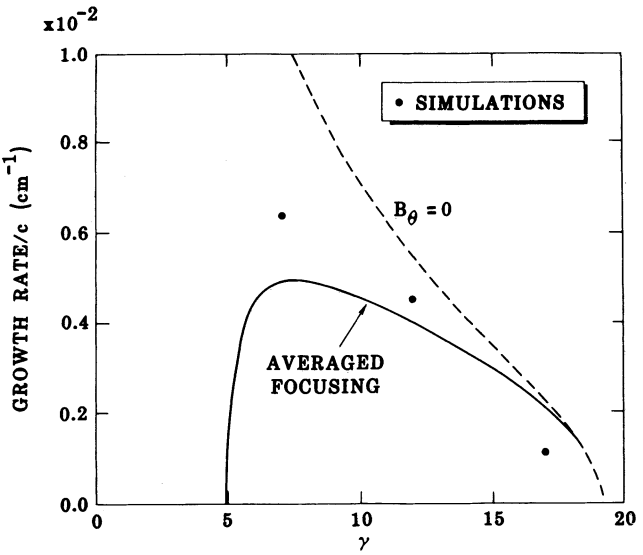

FIGURE 8 Growth rates of the $l = 20$ negative-mass mode on a 10-kA beam in a solenoid-lens betatron, plotted versus beam energy. Growth rates are compared to those for a conventional betatron (dashed line) and those obtained using the averaged-focusing approximation (solid line).

betatron in Ref. (15), rather than using Eq. (31). In doing the simulations, we set the beam radius to 2 cm in order to have good resolution of the beam on the simulation mesh. This means that the solenoid field necessary to get a matched beam decreases as the beam energy increases [see Eq. (39)]. Thus the simulation growth rates shown in Fig. 8 do not represent those experienced by an accelerating beam where the solenoid field is kept constant or increased.

As in the 100-A simulations, we find that the high-l growth rates are anomalously large when frequency spread effects are taken into account. Nevertheless, the simulations for $\gamma_0 = 7$, and $\gamma_0 = 12$ both saturate with no loss of current. Plots from the nonlinear stage of these simulations are shown in Fig. 9. There is considerable churning of the beam after these plots were taken, and this stage of the instability is probably not well modeled with a few Fourier modes. The simulation at $\gamma_0 = 17$ was not run long enough to see saturation.

7. SUMMARY AND DISCUSSION

We have presented an analytic model for the negative-mass instability in the solenoid-lens betatron. Restricting the analysis to low toroidal-mode numbers, the effect of the solenoid lenses are averaged using a multiple-length-scale method. The equations obtained are those of the conventional negative-mass dispersion relation with a modified transverse focusing force. The additional transverse focusing introduces a finite negative-mass transition energy below

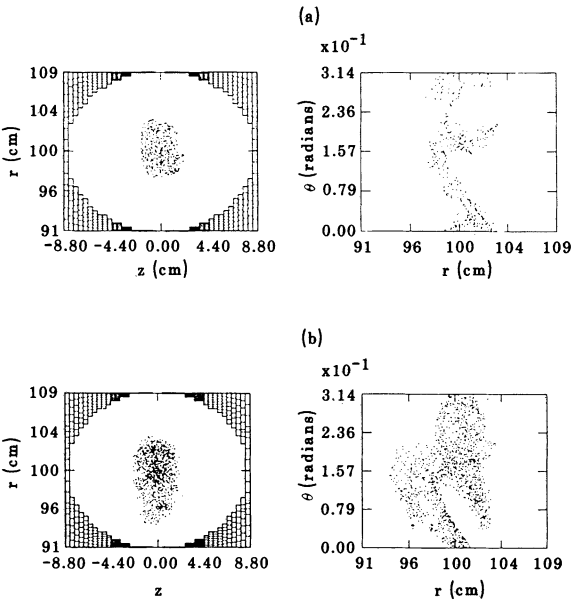

FIGURE 9 Particle plots ($r - z$, $r - \theta$) taken during the nonlinear saturation of the $l = 20$ mode on a 10-kA beam. The beam energy is $\gamma_0 = 7$ in (a), and $\gamma_0 = 12$ in (b).

which the beam is stable. Above this energy, growth rates are suppressed relative to those of the conventional betatron.

The averaged transverse focusing term is used to obtain a kinetic dispersion relation for the solenoid-lens betatron. We find that for a space-charge-dominated equilibrium, it is relatively easy to stabilize the instability with the natural frequency spread due to finite beam radius. This contrasts with other types of betatrons, where an energy spread is needed to produce a significant frequency spread.

Results of three-dimensional PIC code simulations of the IAPBT betatron are in agreement with the predicted stability for low l-numbers, where the averaging procedure is applicable. For a mode number equal to the mode number of the solenoid lenses, on the other hand, we find that the growth rate is anomalously large. In the nonlinear regime, the instability exhibits a classical wave-breaking saturation mechanism leading to some loss of current.

The prediction of a finite negative-mass transition energy is borne out by the simulation results even for large l-numbers. Thus, the IAPBT betatron is predicted to be stable at its injection energy even in the absence of particle frequency spread.

High-current simulations at high mode number show large growth rates comparable to what one would obtain in the absence of any toroidal field (i.e., a conventional betatron). However, no current loss is observed during the nonlinear saturation of the instability.

Finally, we comment briefly on the effect of straight sections on beam stability.

The experimental device at UNM has a racetrack shape (see Fig. 1). In the straight sections, the coupling of longitudinal and transverse beam motion that produces the negative-mass effect disappears. The effect of straight sections on the negative-mass-instability growth rate has been examined analytically and numerically.[18] It is found that, for a given real frequency, the straight sections result in some reduction in growth rate when compared to a circular device of the same total circumference. Unless the straight sections are very long compared to the curved sections, however, the reduction is typically less than a factor of two.

REFERENCES

1. F. Mako, J. Golden, L. Floyd, K. McDonald, T. Smith, and C. A. Kapetanakos, *IEEE Trans. Nuc. Sci.* **NS-32,** 3027 (1985).
2. H. Ishizuka, G. Lindley, B. Mandelbaum, A. Fisher, and N. Rostoker, *Phys. Rev. Lett.* **53,** 266 (1984).
3. H. Ishizuka, J. Saul, A. Fisher, and N. Rostoker, *Proc. 6th International Conference on High-Power Particle Beams,* p. 722, Kobe, Japan, (1986).
4. A. A. Mondelli and C. W. Roberson, *Part. Accel.* **15,** 221 (1984).
5. S. Humphries, Jr. and D. M. Woodall, *Bull. Am. Phys. Soc.* **28,** 1054 (1983).
6. S. Humphries, Jr. and L. K. Len, *J. Appl. Phys.*, **62,** 1568 (1987).
7. D. W. Kerst and R. Serber, *Phys. Rev.* **60,** 53 (1941).
8. R. W. Landau and V. K. Neil, *Phys. Fluids* **9,** 2412 (1966).
9. B. B. Godfrey and T. P. Hughes, *Phys. Fluids* **28,** 669 (1985).
10. P. Sprangle and D. Chernin, *Part. Accel.* **15,** 35 (1984).
11. D. Chernin, *Phys. Fluids* **29,** 556 (1986).
12. J. D. Lawson, "The Physics of Charged Particle Beams", Clarendon, Oxford (1978).
13. J. Struckmeier and M. Reiser, *Part. Accel.* **14,** 227 (1984).
14. D. L. Dobroff, *IRE Trans. Electron Devices* **ED-6,** 68 (1959).
15. B. B. Godfrey and T. P. Hughes, *Part. Accel.* **21,** 173 (1987).
16. H. S. Uhm, R. C. Davidson, and J. J. Petillo, *Phys. Fluids,* **28,** 2537 (1985).
17. T. P. Hughes and B. B. Godfrey, *IEEE Trans. Nuc. Sci.* **NS-32,** 2498 (1985).
18. T. P. Hughes and B. S. Newberger, *Bull. Am. Phys. Soc.* **30,** 1534 (1985).